Real-Time FTIR and *in Situ* Rheological Studies on the UV Curing Kinetics of Thiol-ene Polymers

Bor-Sen Chiou and Saad A. Khan*

Department of Chemical Engineering, North Carolina State University, Raleigh, North Carolina 27695-7905

Received June 13, 1997; Revised Manuscript Received August 25, 1997[⊗]

ABSTRACT: Real-time FTIR spectroscopy and *in situ* dynamic rheology were used to characterize the UV curing kinetics of a thiol-ene system containing trimethylolpropane tris(2-mercaptoacetate) and trimethylolpropane diallyl ether. The combination of these two techniques offered a powerful approach for monitoring changes in the chemical and rheological properties of the system during UV curing. Comparable gel times were independently obtained from both FTIR spectroscopy and rheology, thereby validating the comparison of data obtained from each method. The thiol conversion determined from FTIR spectroscopy was correlated with the elastic modulus obtained from rheology. The conversion increased very rapidly during the initial stages of UV curing. However, the elastic modulus did not have an appreciable value until after 65% of the thiol functional groups have reacted, following which the elastic modulus increased at a rapid rate. From the Flory−Stockmayer theory of gelation, the critical thiol conversion at the gel point was determined to be 0.71. This indicated that the elastic modulus had an appreciable value only when the sample is close to its gel point, consistent with the step growth kinetics of the polymerization reaction. From the conversion data, the photoinitiated thiol-ene reaction was determined to be a second-order reaction. This second-order behavior was inconsistent with the termination mechanisms currently found in literature. A possible reason for such a discrepancy is discussed.

Introduction

The rapid growth of the UV curing industry over the past two decades has stimulated the development of new techniques for analyzing the UV curing process. However, there still lacks a fundamental understanding of many issues associated with UV curing. For example, the relationship between how the curing conditions and the molecular architecture of the monomers affect the final material properties of the cured polymer is not well understood. As a consequence, formulating UV curable systems for the desired properties is mostly done on an empirical basis. To improve understanding of the UV curing process, many studies have focused on characterizing the polymerization kinetics by using a variety of analytical techniques.

Some of the techniques that have been used for kinetic studies on UV curable systems include differential photocalorimetry (DPC),[1−4] dilatometry,[5,6] and Fourier transform infrared (FTIR) spectroscopy.[7,8] Among these techniques, FTIR spectroscopy is the only one able to monitor the specific changes in chemistry during UV curing. This technique provides a fingerprint of the chemical groups present initially in the monomers before reaction and the subsequent changes in chemistry during curing. The FTIR data can be used to directly determine the rate of polymerization by analyzing the decrease in the infrared absorbances of the reacting functional groups. FTIR spectroscopy can also measure the reactant conversion more accurately than either DPC or dilatometry. This is accomplished by monitoring the absorbances of the functional groups before and after UV curing.

Until recently, however, most FTIR studies on UV curing systems have not been done in real-time. The sample is first irradiated for a certain amount of time outside the FTIR spectrometer and then placed in the spectrometer sample chamber for analysis. One of the problems with such an approach is that the sample may become different from the one obtained directly after irradiation. This is due to dark curing, which may occur during the few seconds required to place the sample in the sample chamber. It is therefore desirable to utilize a real-time infrared spectroscopy technique to monitor UV curing. This was initially accomplished on a dispersive infrared spectrometer by Decker et al.[9,10] However, they monitored only a single wavelength, corresponding to the reacting functional group, for determining the rate of polymerization. No stable peak was used as an internal standard to correct for possible artifacts, such as sample shrinkage, that may arise during the experiment. In order to resolve this issue, real-time techniques have recently been applied to an FTIR spectrometer.[11−14] Here, the entire spectrum can be obtained in only a few seconds, thereby allowing an internal standard to be used when analyzing the FTIR data.

Together with FTIR spectroscopy, rheology is another powerful tool that can be used to characterize the UV curing kinetics. Rheological properties measured during UV curing reflect the kinetics of the evolving microstructure, which is due to the formation of cross-links. The extent and density of these cross-links ultimately determine the final mechanical properties of the fully cured polymer. There has been a lack of studies that focus on measuring the rheological properties during UV curing itself because of the lack of an *in situ* technique. Instead, most studies have dealt with measuring the mechanical properties of the fully cured polymer.[7,15,16] However, evolving rheological properties, when measured under different UV curing conditions, can be used to understand and optimize the cross-linking process. In previous studies,[17,18] we have established the feasibility of using an *in situ* rheological technique for characterizing the dynamic rheological behavior of materials during UV curing.

* To whom correspondence should be addressed. Phone: 919-515-4519. Fax: 919-515-3465. E-mail: khan@che.ncsu.edu.

[⊗] Abstract published in *Advance ACS Abstracts,* November 1, 1997.

S0024-9297(97)00865-6 CCC: $14.00

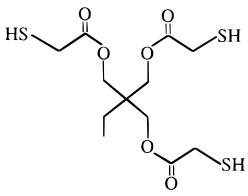

Trimethylolpropane tris(2-mercaptoacetate)

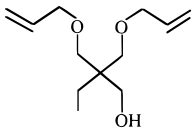

Trimethylolpropane diallyl ether

Figure 1. Schematic representation of the monomers used in the formulation of the thiol-ene system.

In this study, we exploit the advantages of both real-time FTIR spectroscopy and *in situ* rheology to monitor the UV curing of a thiol-ene system. This system consists of trimethylolpropane tris(2-mercaptoacetate) and trimethylolpropane diallyl ether (Figure 1). We have constructed an apparatus that enabled us to perform real-time FTIR experiments on samples of controlled thicknesses and measure overall reactivity throughout the sample, a feature missing from the earlier studies. This allows us to correlate directly the changes in chemistry and conversion obtained from FTIR spectroscopy to real-time rheological measurements. A relationship between macroscopic properties, such as the moduli obtained from rheology, and molecular properties, such as the conversion obtained from FTIR spectroscopy, is vital for providing physical insight into the fundamental processes occurring during UV curing.

Experimental Section

Materials. A stoichiometric mixture of a trifunctional thiol, trimethylolpropane tris(2-mercaptoacetate), with a difunctional allyl monomer, trimethylolpropane diallyl ether, was used for all our experiments. Both monomers were purchased from Aldrich Chemicals and used as received. Hydroquinone was added to the thiol and allyl monomer mixture in order to prevent premature polymerization. This was then mixed thoroughly for 5 min. The hydroquinone was also purchased from Aldrich Chemicals and used as received. A commercial photoinitiator, Esacure TZT (Sartomer Inc.), which contains a blend of methylbenzophenones, was then added to the mixture. The mixture was stirred for an additional 5 min before it was placed in either the FTIR spectrometer or the rheometer. The final concentrations of the photoinitiator and the hydroquinone in the mixture were 1% and 0.5% by weight of monomers, respectively.

Real-Time FTIR Spectroscopy. The apparatus for obtaining the real-time IR spectra during UV curing consisted of a liquid light guide and two 25 mm × 4 mm BaF_2 crystals. The schematic of the apparatus is shown in Figure 2. UV radiation from a 200 W Oriel mercury lamp was introduced into the FTIR spectrometer sample chamber by the flexible light guide. A wavelength of 365 nm was maintained using a narrow band interference filter. The radiation intensity was attenuated by using neutral density filters and was held constant at 0.10 mW cm^{-2}. An International Light 1400A radiometer was used to measure the radiation intensity. The liquid light guide was positioned at a distance of 6 mm from the BaF_2 crystals to ensure total UV radiation coverage of the crystals. The light guide was also tilted at an angle of 15° so that it did not block the path of the IR beam. The thiol-ene

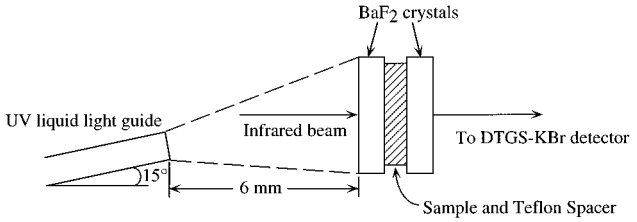

Figure 2. Schematic representing the FTIR apparatus used to conduct real-time UV curing measurements. The sample is sandwiched between two BaF_2 crystals held apart by a Teflon O-ring spacer. The UV liquid light guide is positioned so that the UV radiation covers the entire BaF_2 crystal but does not block the IR beam.

sample was sandwiched between the two crystals using a 50 μm Teflon O-ring spacer. This unit was placed in a Spectra-Tech Presslock Holder and then inserted inside the FTIR spectrometer sample chamber.

This real-time FTIR technique offers several advantages over others reported in literature. First, spacers with different thicknesses can be used to control the sample thickness, unlike other FTIR techniques[13,14] that do not have the capability for accurately controlling sample thicknesses. This allowed the sample to be monitored under the same conditions as those present in the rheological experiments, where the sample is sandwiched between plates held at a known distance apart. Furthermore, the BaF_2 crystals used in our approach have a longer lifetime than the KBr crystals used by others[11] since the former is not hygroscopic and will not fog up when exposed to the moisture in the air.

The FTIR experiments were performed using a Nicolet Magna-IR System 750 spectrometer with a DTGS-KBr detector. Each of the IR spectra obtained from the spectrometer is an average of five scans, each with a resolution of 4 cm^{-1}; the time to acquire each spectra was 10 s. The spectra were obtained one after another in order to ensure that the UV curing process was analyzed in real time. Either the C═C stretching vibrations of the allyl functional groups at 1646 cm^{-1} or the S—H stretching vibrations of the thiol functional groups at 2570 cm^{-1} can be used to calculate conversions. We chose the thiol absorption because it was stronger than the allyl absorption. The aromatic out-of-phase C—H deformation vibration from the methylbenzophenone photoinitiators at 830 cm^{-1} was used as an internal standard since this peak remained unchanged during the course of the experiment. All experiments were performed at 25 °C.

The conversion of the thiol (2570 cm^{-1}) functional group at any time can be calculated by first integrating the unreacted thiol peak at the start of the experiment. At a subsequent time t, the area of the peak can be integrated and the conversion at that time can be determined as follows (19):

$$x(t) = \frac{A(0) - A(t)}{A(0)} \tag{1}$$

where $x(t)$ is the conversion at time t, $A(0)$ is the normalized area (with respect to 830 cm^{-1}) of the initial thiol peak, and $A(t)$ is the normalized area of the thiol peak at time t.

Dynamic Rheology. *In situ* monitoring of the UV curing process was conducted using a Rheometrics mechanical spectrometer (RMS 800) in conjunction with specially designed parallel plate fixtures. A description of these fixtures is given elsewhere.[18] The same 200 W Oriel mercury lamp used in the FTIR experiments was used for the rheological experiments. A narrow band interference filter maintained the wavelength of the incident UV radiation at 365 nm, while neutral density filters attenuated the radiation intensity. The intensity was measured prior to each experiment by using the radiometer and held constant at 0.10 mW cm^{-2}, as in the FTIR experiments. Radial variation in the incident radiation intensity was adjusted to less than ~7% in all cases. The sample thickness was maintained at 0.05 mm and experiments were performed at 25 °C, thereby ensuring that both the rheological and the FTIR experiments were performed under the same conditions.

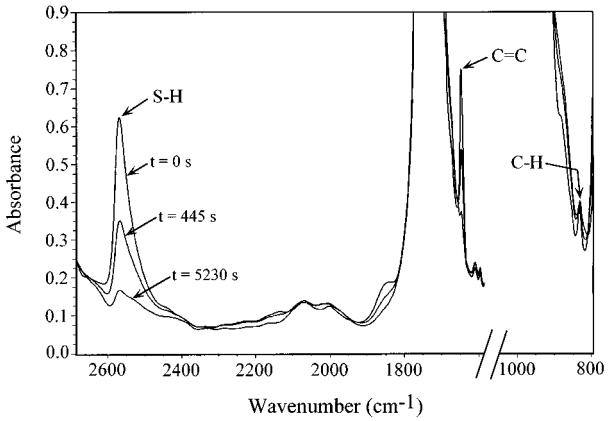

Figure 3. Typical IR spectrum shown for three different UV exposure times. The S—H (2570 cm^{-1}) and C═C (1646 cm^{-1}) peaks are decreasing with time, while the aromatic out-of-phase C—H (830 cm^{-1}) peak does not change during UV curing. The thiol (S—H) peak is monitored to calculate the conversion, while the C—H peak is used as the internal standard.

A dynamic rheological technique, Fourier transform mechanical spectroscopy (FTMS),[21,22] was used for monitoring the UV curing process. In a conventional dynamic rheological experiment, a sinusoidal strain deformation, γ, is applied to the sample at a frequency, ω, and a strain amplitude, γ_0:[20]

$$\gamma = \gamma_0 \sin(\omega t) \tag{2}$$

The resulting stress (τ_{xy}) on the sample is then measured and is given as[20]

$$\tau_{xy} = G'\gamma_0 \sin(\omega t) + G''\gamma_0 \cos(\omega t) \tag{3}$$

The stress can be decoupled into two parts, one in phase with the deformation, characterized by the elastic modulus, G', and one out of phase with the deformation, characterized by the viscous modulus, G''. The elastic modulus measures the amount of energy stored by the material during one oscillation cycle, while the viscous modulus measures the amount of energy dissipated during the same cycle. The elastic modulus is particularly sensitive to the microstructure of the material. The FTMS technique differs from conventional dynamic experiments in that the applied strain is a summation of several strain deformations, i.e., $\gamma = \sum\gamma_i \sin(\omega_i t)$. This approach enables simultaneous measurement of the evolving dynamic moduli at several frequencies during the course of UV curing. The fundamental frequency ($\omega_i = \omega_1$) was set at 1 rad/s for our experiments, while the higher harmonics were chosen to be 5, 10, 70, and 100 rad/s. It required 25 s to complete a set of the moduli measurements at these frequencies. The use of a low intensity ensured that rheological properties remained unchanged during this time frame. Strains of 10% were chosen for each frequency, with the summation of the strains being well below the linear viscoelastic regime of the material.

Results and Discussion

Thiol Conversion and Rheological Behavior. The infrared spectrum of the thiol-ene system for three different UV exposure times is shown in Figure 3. At the beginning of the curing process, both the thiol (2570 cm^{-1}) and allyl (1646 cm^{-1}) peaks are distinct. As curing progresses, the peaks begin to shrink in size as more of the functional groups react to form a cross-linked network. Toward the end of the process, the peaks have decreased to almost zero absorbance since most of the functional groups have already reacted. The aromatic out-of-phase C—H deformation peak (830 cm^{-1}) did not change during the course of the reaction and was used as the internal standard. Note that the area under the thiol peak (2570 cm^{-1}) is larger than the area under the allyl peak (1646 cm^{-1}). We therefore use the changes in the area under the thiol peak in order to calculate conversions.

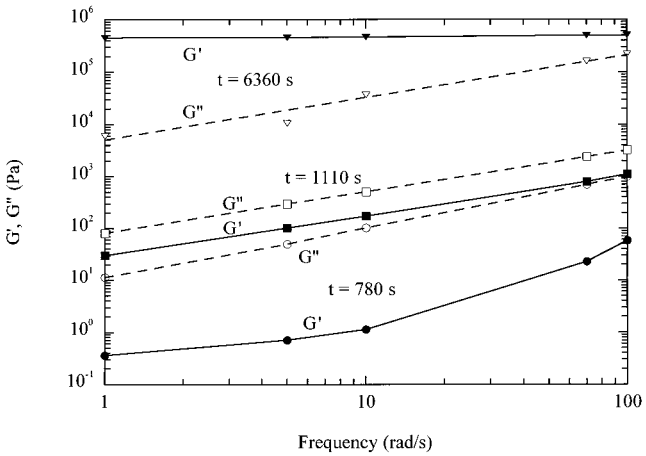

Figure 4. Elastic (G') and viscous (G'') moduli as a function of frequency for three different UV exposure times. During the early stages of UV curing (t = 780 s), the sample is still a viscous liquid. At t = 1110 s, the sample has reached its gel point. Toward the end of the reaction (t = 6360 s), the sample has become a highly cross-linked gel.

In Figure 4, we have plotted the elastic and viscous moduli as a function of frequency for three different UV exposure times. The evolving elastic (G') and viscous (G'') moduli during UV curing measure the buildup of microstructure due to the formation of chemical cross-links. During the initial stages of the reaction (t = 780 s), the viscous modulus is much greater than the elastic modulus throughout the entire frequency range. This indicates that the sample is still a viscous liquid. When the sample is exposed to 1110 s of UV radiation, both the elastic and viscous moduli have the same dependence on the frequency of oscillation. Since Figure 4 is plotted on a log—log scale, this means that the elastic and viscous moduli exhibit the same power-law behavior with respect to the frequency of oscillation (G', $G'' \sim \omega^n$). It has been shown by Winter and Chambon[23,24] that a material exhibiting this behavior is at its gel point. The gel point in a chemically cross-linking system marks the transition from a viscous liquid to a viscoelastic gel and occurs when a macromolecular cluster is produced that is large enough to span the entire sample size. When the sample is further exposed to UV radiation (t = 6360 s), the elastic modulus becomes greater than the viscous modulus throughout the frequency range and also independent of frequency, both of which are characteristics of a highly cross-linked gel. Note that the elastic modulus increases by up to 6 orders of magnitude during the UV curing process.

An alternate way of visualizing the evolving elastic and viscous moduli is by plotting the moduli as a function of UV exposure time for a specific frequency. Figure 5 shows such a plot where the frequency of oscillation is 10 rad/s. Initially, the viscous modulus is larger than the elastic modulus, indicating that the sample is still liquid-like. Both moduli increase during the course of UV curing, with the elastic modulus increasing at a faster rate than the viscous modulus. Eventually, the elastic modulus becomes equal to the viscous modulus after 1500 s of UV exposure. Toward the end of the UV curing process, the sample has become a highly cross-linked gel with an elastic modulus greater than the viscous modulus.

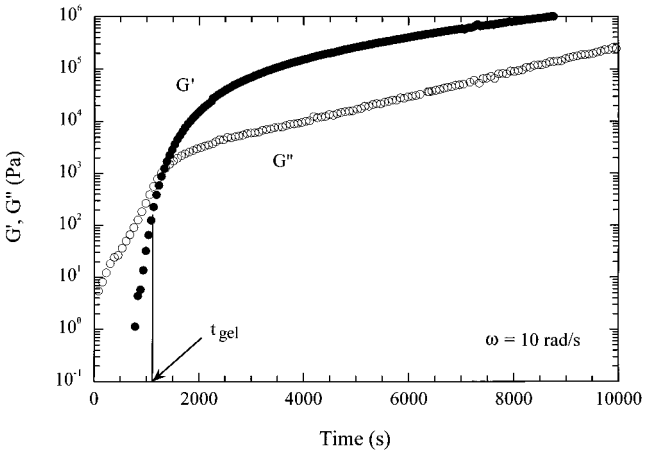

Figure 5. Evolving elastic (G') and viscous (G'') moduli during UV curing obtained by using the *in situ* rheological technique. Here, the frequency of oscillation is 10 rad/s.

In order to determine the efficacy of correlating data obtained from FTIR spectroscopy and rheology, we first examined the gel time, the time needed in order to reach the gel point, obtained by each of the techniques. We can determine the gel time from rheology by utilizing the Winter−Chambon criterion (i.e., G', $G'' \sim \omega^n$ or tan $\delta \equiv G''/G' =$ constant).[23,24] Using this criterion, we find the gel time for our system to be 1170 ± 80 s. In order to determine the gel time from FTIR spectroscopy, we use the classic Flory−Stockmayer theory of gelation to obtain the critical thiol conversion at the gel point. Once we determine the time required for the sample to reach the critical conversion at gel point, we can then compare it with the gel time determined by rheology. The critical thiol conversion at the gel point, x_c, from the Flory−Stockmayer theory of gelation is expressed as[25]

$$x_c = \frac{1}{[r(f_{thiol} - 1)(f_{allyl} - 1)]^{1/2}} \quad (4)$$

where r is the stoichiometric ratio of the thiol to allyl functional groups, f_{thiol} is the functionality of the thiol, and f_{allyl} is the functionality of the allyl monomer. For a trifunctional thiol and a difunctional allyl monomer, the critical conversion at the gel point is 0.71. Since we know from rheology that the gel time for our system is 1170 ± 80 s, we would like to see if the conversion at 1170 s, determined from FTIR spectroscopy, is indeed 0.71. The thiol conversion at 1170 s was found to be 0.71 ± 0.01, matching the critical conversion predicted by the Flory−Stockmayer theory. The agreement between the gel times obtained from FTIR spectroscopy and rheology further validates the use of dynamic rheology, in conjunction with the Winter−Chambon criterion, as an accurate method for determining the gel point. The agreement also means that it is valid to compare the FTIR data with the rheology data.

Utilizing FTIR and rheological techniques, we measured the thiol conversion and elastic modulus, respectively, as a function of the UV exposure time. We have plotted the thiol conversion and the elastic modulus as a function of time in Figure 6. During the initial stages of UV curing, the thiol conversion increases very rapidly and reaches a value of ~0.7 after 1000 s. During this period of time, the elastic modulus still does not have an appreciable value. The elastic modulus begins to increase only after 1000 s of UV exposure but increases very rapidly thereafter. In order to explain this behavior, we have to examine the gel point of the sample. From the Flory−Stockmayer theory of gelation, we found the critical conversion at the gel point for our thiol-ene system to be 0.71. This indicates that the reaction has to proceed to a high enough conversion, one which is close to the critical conversion at the gel point, in order for the elastic modulus to be detectable. Similar results have been obtained for a PDMS system,[26] where an appreciable modulus did not appear until after 55% of the silane functional groups have reacted. Note that the greatest rate of increase of the thiol conversion does not necessarily have to match the greatest rate of increase of the elastic modulus.

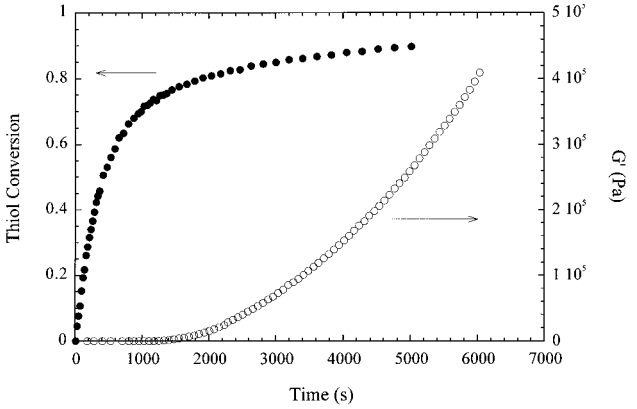

Figure 6. Thiol conversion and dynamic elastic modulus, G', plotted as a function of the UV exposure time. The thiol conversion increased very rapidly during the initial stages of the reaction. An appreciable elastic modulus could only be detected near the gel point after a considerable fraction of the thiol functional groups have reacted.

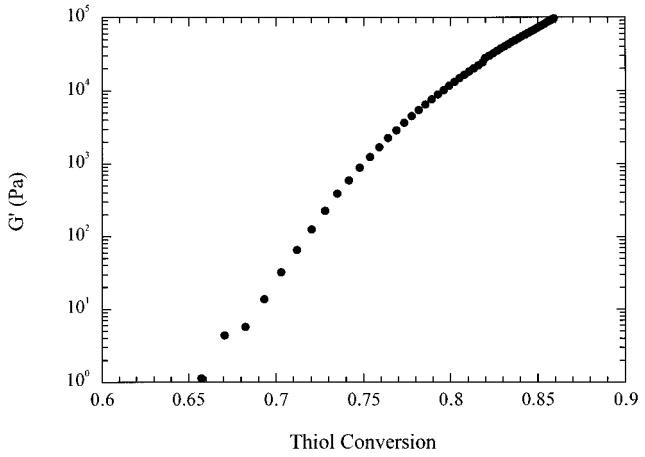

Figure 7. Correlation of the elastic modulus with the thiol conversion. This shows clearly that once the elastic modulus is detected, it increases at a rapid rate. The elastic modulus increases by 5 orders of magnitude for a 20% increase in conversion from 65% to 85%.

We have plotted the elastic modulus as a function of the thiol conversion in Figure 7. Two features are apparent from this plot. First, the modulus is almost negligible until a conversion of 0.65, close to the gel point, is reached. Second, the elastic modulus is extremely sensitive to the material microstructure for conversions exceeding 0.65. In fact, the modulus increases by 5 orders of magnitude for only a 20% increase in conversion from 65% to 85%. These features of the elastic modulus are consistent with the step-growth polymerization mechanism suggested for thiol-ene systems. Because of this mechanism, as chemical crosslinking progresses, many small but separate "clusters"

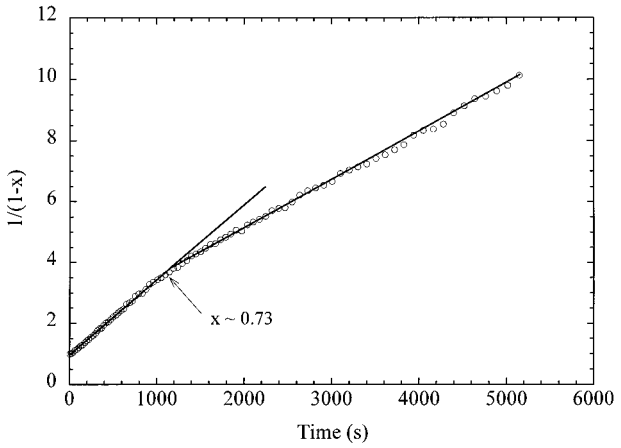

Figure 8. Plot of $1/(1 - x)$ as a function of the UV exposure time. This plot indicates that the trimethylolpropane tris(2-mercaptoacetate)/trimethylolpropane diallyl ether reaction is a second-order reaction throughout the UV curing process, but the rate constant changes once the system has passed the gel point (conversion ~0.7).

or "chains" are being formed. These small clusters have very short relaxation times compared to the time scales of the rheological experiment, which in this case range from 1 to 0.01 s (e.g., frequencies of 1−100 rad/s). Therefore, we are unable to detect an appreciable elastic modulus during the early stages of the reaction because the clusters relax faster than the time scales of the imposed deformation.[27] It is only near the gel point that cross-linking between the clusters starts to occur. Relaxation times become comparable to the time scales of the imposed deformation and increase rapidly as the clusters merge to produce a gel network. Correspondingly, an appreciable elastic modulus is detected only near the critical conversion, whereupon the modulus exhibits a sharp increase with conversion.

Thiol-ene Reaction Order. The thiol conversion data was also used to determine a reaction order for the photoinitiated thiol-ene reaction. By assuming a rate expression for the reaction and then using the integral method to analyze the kinetic data, we can obtain the order of the reaction. For our thiol-ene system, we assumed a second-order reaction:[28]

$$\frac{dx}{dt} = k(1 - x)^2 \tag{5}$$

where x is the thiol conversion, t is the time, and k is the rate constant. This expression can then be integrated from the beginning of the reaction ($t = 0$ s, $x = 0$) to a time t and a conversion x:

$$\frac{1}{(1 - x)} = kt + 1 \tag{6}$$

Therefore, a plot of $1/(1 - x)$ as a function of time would result in a straight line with the slope equal to the rate constant. Such a plot is shown in Figure 8, where we find that $1/(1 - x)$ increases linearly with time up to a UV exposure time of ~1200 s. After this point, the relationship is still linear but the slope of the line changes. The thiol conversion corresponding to the UV exposure time when the slope change occurs is ~0.73, which is close to the critical conversion at the gel point. These results seem to indicate that the reaction order remains second-order throughout the cross-linking process; however, the rate constant changes once the system has passed the gel point. A possible explanation

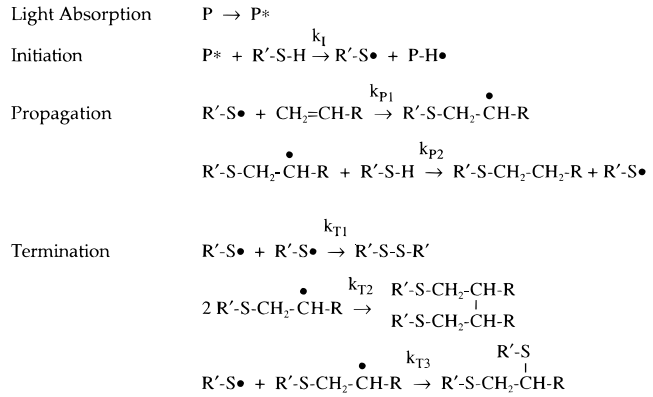

Figure 9. Schematic of the suggested mechanism for the photoinitiated thiol-ene reaction. The reaction propagates via free radicals but exhibits step-growth kinetics. Rate constants for each of the proposed steps are also shown.

for the behavior after the gel point may lie in the restricted mobility of the radical species that have been occluded onto the network. As the cross-linked network grows larger and larger, more of the radical species become occluded onto the network. This severely reduces their mobility since they are constrained by the network structure. The reduced mobility then results in longer times for the radical species to react and hence a smaller rate or a lower than expected conversion.

A mechanism for the photoinitiated thiol-ene reaction has been suggested in the literature and a schematic of this mechanism is shown in Figure 9.[29] The photoinitiator (P) first absorbs UV radiation to produce an excited species (P*). This species then abstracts a hydrogen from a thiol to produce a thiyl radical, R′S•. Propagation then occurs in two steps: first, the thiyl radical adds to the olefin to produce an intermediate thioether carbon radical, R′SCH$_2$C•HR, and then the thioether carbon radical abstracts a hydrogen from another thiol to regenerate the thiyl radical. Termination for this reaction is believed to occur by one of three radical−radical recombinations possible: between two thiyl radicals, between two thioether carbon radicals, or between a thioether carbon and a thiyl radical. However, the exact termination mechanism for thiol-ene reactions is still obscure.[30]

We have formulated rate expressions for each of the suggested termination mechanisms in order to check which, if any, of the three termination mechanisms are consistent with the reaction order determined for our system. Since we have used the thiol conversion to determine the reaction order, we will have to obtain an expression for the overall rate of disappearance of thiol. The final overall expressions for the rate of disappearance of thiol for each of the termination mechanisms have been determined and appear in the Appendix. If we assume that termination occurs by the recombination of two thiyl radicals ($k_{T2} = k_{T3} = 0$) (see Figure 9), the rate expression for the disappearance of thiol will have a one-half-order dependence on the thiol concentration and a first-order dependence on the allyl concentration. Since we used stoichiometric amounts of the thiol and allyl monomers, we can further reduce the rate expression to a three-half-order dependence on the thiol concentration. For a termination mechanism involving the recombination of two thioether carbon radicals ($k_{T1} = k_{T3} = 0$), the rate expression for the disappearance of thiol will also have a three-half-order dependence on the thiol concentration. Finally, if termination occurs by the recombination of a thiyl and a thioether carbon

radical ($k_{T1} = k_{T2} = 0$), the rate expression will not have a simple dependence on the thiol and allyl monomer concentrations. Therefore, none of the termination mechanisms suggested in the literature are consistent with the overall second-order reaction rate obtained from our FTIR data.

We can account for the second-order dependence of the rate expression on the thiol concentration (or thiol conversion) by proposing an alternate termination mechanism involving a reaction between the thiyl radical and possibly some impurities in the sample:

$$R'S^{\bullet} + M \xrightarrow{k_{T4}} R'SM^{\bullet} \quad (7)$$

$$R'SM^{\bullet} + R'SM^{\bullet} \xrightarrow{k_{T5}} R'SMMSR' \quad (8)$$

where M represents the impurities and k_{T4} and k_{T5} are rate constants for the termination steps. In fact, a study[31] has shown that in the presence of a trace amount of impurity, such as butadiene, the termination mechanism for a thiol-ene reaction switches from the recombination of thiyl radicals to a mechanism involving the butadiene. If we use this new termination mechanism to determine the rate expression for the disappearance of thiol, the rate expression will have a first-order dependence on the thiol concentration and a first-order dependence on the allyl concentration (see Appendix). Since we used stoichiometric amounts of thiol and allyl monomers, the rate expression can be reduced to a second-order dependence on the thiol concentration, which is then consistent with the obtained FTIR data. While the presence of impurities cannot be ruled out in our system, we find FTIR data (not shown) on conversion versus time for thiol and allyl functional groups to overlap with each other. This suggests that any impurities, if present, do not interfere with the reaction of these functional groups with each other. We would also like to emphasize that our proposed mechanism is only one *possible scenario* that is consistent with the experimental data. Further work is necessary in order to determine more precisely the reason for the discrepancy between the experimental and predicted reaction order.

Conclusions

We have designed an apparatus that enabled us to perform real-time FTIR experiments for characterizing the UV curing of a trimethylolpropane tris(2-mercaptoacetate)/trimethylolpropane diallyl ether system. From these FTIR experiments, we obtained the thiol conversion as a function of UV exposure time. We also monitored the evolving elastic and viscous moduli during UV curing by using *in situ* rheology. We found the gel time obtained from FTIR spectroscopy to match very closely with the gel time determined from rheology. This validated the combined use of FTIR spectroscopy with rheology, a powerful approach to probe the chemical and rheological changes during UV curing.

We correlated the thiol conversion with the elastic modulus in order to compare changes in the molecular and macroscopic properties of the thiol-ene system during the curing process. We found that the conversion increased very rapidly during the initial stages of UV curing. However, the elastic modulus did not reach an appreciable value until the thiol conversion was close to the critical gel point, following which the elastic modulus increased at a very rapid rate. For an increase in conversion from 0.65 to 0.85, the elastic modulus increased by 5 orders of magnitude, showing the sensitivity of the elastic modulus to the developing microstructure.

We found the thiol-ene reaction to behave as a second-order reaction. However, the rate constant decreased following the gel point. A possible explanation for this may be that the cross-linked network formed after the gel point restricted the mobility of the occluded radical species. This resulted in longer reaction times and thus a smaller rate constant or lower than expected conversion. We also found that the rate expressions formulated for each of the different termination mechanisms suggested in the literature were inconsistent with the reaction order experimentally obtained for our system. In order to account for this inconsistency, we proposed an alternate termination mechanism.

Acknowledgment. We thank the Petroleum Research Fund, administered by the American Chemical Society, and a GAANN Fellowship (NSF) for providing financial support for this work. The authors would also like to thank Profs. Gregory L. Baker (Chemistry, Michigan State) and Mohan Srinivasarao (Textiles, North Carolina State) for their comments and suggestions during the preparation of this manuscript.

Appendix

We will derive a rate expression for the case where termination occurs by recombination of two thiyl radicals ($k_{T2} = k_{T3} = 0$) (see Figure 9) in detail and then just present the final rate expressions derived from the other termination mechanisms. We begin by obtaining the overall rate expression for the disappearance of thiol:

$$\frac{d[R'SH]}{dt} = -k_I[P^*][R'SH] - k_{P2}[R'SH][R'SCH_2C^{\bullet}HR] \quad (1)$$

Applying the steady-state approximation to the overall rate expression for the thioether carbon radical gives us

$$\frac{d[R'SCH_2C^{\bullet}HR]}{dt} = k_{P1}[R'S^{\bullet}][CH_2{=}CHR] - k_{P2}[R'SH][R'SCH_2C^{\bullet}HR] \approx 0 \quad (2)$$

We then apply the steady-state approximation to the overall rate expression for the thiyl radical:

$$\frac{d[R'S^{\bullet}]}{dt} = k_I[P^*][R'SH] - k_{P1}[R'S^{\bullet}][CH_2{=}CHR] + k_{P2}[R'SH][R'SCH_2C^{\bullet}HR] - 2k_{T1}[R'S^{\bullet}]^2 \approx 0 \quad (3)$$

Adding eqs 2 and 3 and solving for the thiyl radical concentration give us

$$[R'S^{\bullet}] = \left[\frac{k_I}{2k_{T1}}[R^*][P'SH]\right]^{1/2} \quad (4)$$

Substituting eq 4 back into eq 2 and solving for the thioether carbon radical concentration give us

$$[R'SCH_2C^{\bullet}HR] = \frac{k_{P1}k_I^{1/2}}{k_{P2}(2k_{T1})^{1/2}}[P^*]^{1/2}\frac{[CH_2{=}CHR]}{[R'SH]^{1/2}} \quad (5)$$

We then substitute eq 5 back into eq 1 and assume that $k_I[P^*][R'SH] \ll k_{P2}[R'SH][R'SCH_2C^{\bullet}HR]$. This gives us

$$\frac{d[R'SH]}{dt} = -\frac{k_{P1}k_I^{1/2}}{(2k_{T1})^{1/2}}[P^*]^{1/2}[R'SH]^{1/2}[CH_2{=}CHR] \quad (6)$$

[P*] can be replaced by $\alpha[P]$, where α is a proportionality constant, to obtain the desired final rate expression:

$$\frac{d[R'SH]}{dt} = -\frac{k_{P1}k_I^{1/2}\alpha^{1/2}}{(2k_{T1})^{1/2}}[P]^{1/2}[R'SH]^{1/2}[CH_2{=}CHR] \quad (7)$$

A similar analysis for the remaining termination mechanisms gives the following rate expressions:

(i) Termination by recombination of two thioether carbon radicals ($k_{T1} = k_{T3} = 0$)

$$\frac{d[R'SH]}{dt} = -\frac{k_{P2}k_I^{1/2}\alpha}{(2k_{T2})^{1/2}}[P][R'SH]^{3/2} \quad (8)$$

(ii) Termination by recombination of thiyl and thioether carbon radicals ($k_{T1} = k_{T2} = 0$)

$$\frac{d[R'SH]}{dt} = -\frac{[R'SH]}{2}\left[\frac{k_I^2\alpha^2[P]^2}{4} + \frac{4k_Ik_{P1}k_{P2}\alpha[P][CH2{=}CHR]}{k_{T3}}\right]^{1/2} \quad (9)$$

(iii) Proposed termination mechanism involving thiyl radical and M

$$\frac{d[R'SH]}{dt} = -\frac{k_Ik_{P1}\alpha[P][R'SH][CH_2{=}CHR]}{k_{T4}[M]} \quad (10)$$

References and Notes

(1) Tryson, G. R.; Shultz, A. R. *J. Polym. Sci., Polym. Phys. Ed.* **1979**, *17*, 2059.
(2) Kloosterboer, J. G.; Lijten, G. F. C. M. *Polymer* **1987**, *28*, 1149.
(3) Hoyle, C. E.; Hensel, R. D.; Grubb, M. B. *Polym. Photochem.* **1984**, *4*, 69.
(4) Hoyle, C. E.; Hensel, R. D.; Grubb, M. B. *J. Polym. Sci., Polym. Chem. Ed.* **1984**, *22*, 1865.
(5) Bowman, C. N.; Peppas, N. A. *J. Appl. Polym. Sci.* **1991**, *42*, 2013.
(6) Kinkelaar, M.; Lee, L. J. *J. Appl. Polym. Sci.* **1992**, *45*, 37.
(7) Jacobine, A. F.; Glaser, D. M.; Grabek, P. J.; Mancini, D; Masterson, M.; Nakos, S. T.; Rakas, M. A.; Woods, J. G. *J. Appl. Polym. Sci.* **1992**, *45*, 471.
(8) Nishikubo, T.; Kameyama, A.; Sasano, M.; Sawada, M. *J. Polym. Sci., Part A: Polym. Chem.* **1993**, *31*, 91.
(9) Decker, C.; Moussa, K. *Macromolecules* **1989**, *22*, 4455.
(10) Decker, C.; Moussa, K. *Makromol. Chem.* **1988**, *189*, 2381.
(11) Udagawa, A.; Sakurai, F.; Takahashi, T. *J. Appl. Polym. Sci.* **1991**, *42*, 1861.
(12) Dietz, J. E.; Elliot, B. J.; Peppas, N. A. *Macromolecules* **1995**, *28*, 5163.
(13) Yang, D. B. *J. Polym. Sci., Part A: Polym. Chem.* **1993**, *31*, 199.
(14) Allen, N. S.; Hardy, S. J.; Jacobine, A. F.; Glaser, D. M.; Yang, B.; Wolf, D. *Eur. Polym. J.* **1990**, *26*, 1041.
(15) Rakas, M. A.; Jacobine, A. F. *J. Adhesion* **1992**, *36*, 247.
(16) Torres-Filho, A.; Neckers, D. C. *J. Appl. Polym. Sci.* **1994**, *51*, 931.
(17) Chiou, B.; English, R. J.; Khan, S. A. *Macromolecules* **1996**, *29*, 5368.
(18) Khan, S. A.; Plitz, I. M.; Franz, R. A. *Rheol. Acta* **1992**, *31*, 151.
(19) Decker, C. In *Radiation Curing: Science and Technology*; Pappas, S. P., Ed.; Plenum Press: New York, 1992; p 135.
(20) Macosko, C. W. *Rheology: Principles, Measurements, and Applications*; VCH Publishers: New York, 1994; Chapter 3.
(21) Holly, E. E.; Venkataraman, S. K.; Chambon, F.; Winter, H. H. *J. Non-Newtonian Fluid Mech.* **1988**, *27*, 17.
(22) In, M.; Prud'homme, R. K. *Rheol. Acta* **1993**, *32*, 556.
(23) Winter, H. H. Gel Point. In *Encyclopedia of Polymer Science and Engineering*; John Wiley & Sons: New York, 1989.
(24) Winter, H. H.; Chambon, F. *J. Rheol.* **1986**, *30*, 367.
(25) Odian, G. *Principles of Polymerization*; John Wiley & Sons: New York, 1991; Chapter 2.
(26) Venkataraman, S. K.; Coyne, L.; Chambon, F.; Gottlieb, M.; Winter, H. H. *Polymer* **1989**, *30*, 2222.
(27) Khan, S. A.; Prud'homme, R. K.; Rabinovitch, E. M.; Sammon, M. J. *J. Non-Cryst. Solids* **1989**, *110*, 153.
(28) Halley, P. J.; Mackay, M. E. *Polym. Eng. Sci.* **1996**, *36*, 593.
(29) Morgan, C. R.; Magnotta, F.; Ketley, A. D. *J. Polym. Sci., Polym. Chem. Ed.* **1977**, *15*, 627.
(30) Jacobine, A. F. In *Radiation Curing in Polymer Science and Technology*; Fouassier, J. B., Rabek, J. F., Eds.; Elsevier Science Publishers Ltd.: New York, 1993; Vol. III, p 219.
(31) Graham, D. M.; Mieville, R. L.; Sivertz, C. *Can. J. Chem.* **1964**, *42*, 2239.

MA9708656